J Fluoresc (2015) 25:465–471
DOI 10.1007/s10895-015-1542-0

ORIGINAL PAPER

Optical Characterization of Normal, Benign, and Malignant Thyroid Tissue: A Pilot Study

M. P. Brandao · R. Iwakura · F. S. Basilio · K. Haleplian · A. S. Ito · L. C. Conti de Freitas · L. Bachmann

Received: 3 December 2014 / Accepted: 23 February 2015 / Published online: 3 March 2015

Abstract Fine-needle aspiration cytology is the standard technique to diagnose thyroid pathologies. However, this method has a high percentage of inconclusive and false-negative results for benign and malignant lesions. Hence, it is important to search for a new method to assist medical evaluation during these surgical procedures. The use of time-resolved fluorescence techniques to detect biochemical composition and tissue structure alterations could help to develop a portable, minimally invasive, and non-destructive method to assist medical evaluation. In this study, we investigated 17 human thyroid samples by absorbance, fluorescence, excitation, and time-resolved fluorescence measurements. This initial investigation has demonstrated that thyroid fluorescence originates from many endogenous fluorophores and culminates in several bands. The fluorescence lifetimes of benign and malignant lesions were significantly different, as attested by analysis of variance using Tukey test with individual confidence level of 98.06 %. Our results suggest that fluorescence lifetimes of benign and malignant lesions can potentially assist diagnosis. After further investigations, fluorescence methods could become a tool for the surgeon to identify differences between normal and pathological thyroid tissues.

Keywords Fluorescence spectroscopy · Fluorescence lifetime · Thyroid tissue · Carcinoma

M. P. Brandao (✉) · K. Haleplian · A. S. Ito · L. Bachmann
Departamento de Física, Faculdade de Filosofia, Ciências e Letras de Ribeirão Preto, Universidade de São Paulo, Av. Bandeirantes 3900, Ribeirão Preto, SP, Brazil 14040-901
e-mail: mpbrandao@gmail.com

R. Iwakura · F. S. Basilio · L. C. C. de Freitas
Departamento de Oftalmo, Otorrino e Cirurgia de Cabeça e Pescoço, Faculdade de Medicina de Ribeirão Preto, Universidade de São Paulo, Av. Bandeirantes 3900, Ribeirão Preto, SP, Brazil 14040-901

Introduction

Thyroid nodules occur frequently, but most of them are benign. At present, fine-needle aspiration (FNA) cytology is the most accepted modality to diagnose thyroid pathologies. However, this method cannot differentiate between benign and malignant follicular lesions clearly, which culminates in high percentage of false-negative results for thyroid injuries, with accuracy ranging from 2 to 37 % [1, 2].

The thyroid has a very complex function. This creates endless controversies regarding cytological and histological analyses, hormone regulation, and surgical procedure (partial or total thyroidectomy). It is difficult to differentiate between hyperplastic nodule (goiter), follicular adenoma, and follicular carcinoma, so new methods that can assist the medical evaluation are necessary. The application of optical methods to characterize the biochemical composition and structure of thyroid pathologies could result in a minimally invasive and non-destructive methodology to detect malignancy in thyroid nodules.

Recently, scientists have evaluated several optical techniques to diagnose pathologies, including thyroid tissue injuries. Optical biopsy by Raman spectroscopy [2], Fourier transform infrared (FTIR) spectroscopy [3], magnetic resonance spectroscopy [4], elastic scattering spectroscopy [5], second-harmonic generation (SHG) microscopy [6], optical coherence tomography [7], and fluorescence spectroscopy [8–10] are among these techniques.

Static fluorescence techniques can assist diagnosis of thyroid injuries [8–11], because they provide marks that can differentiate between health tissue and lesion over a spectral range. Time-resolved fluorescence could also provide diagnostic information about thyroid pathologies [12] and lead to a portable, minimally invasive, and non-destructive method. One advantage of time-resolved fluorescence is that the

fluorescence time decay remains unaltered upon changes in the irradiation intensity of a small volume of the tissue.

In biological systems, endogenous substances like NADH (nicotinamide adenine dinucleotide), flavins (mainly flavin adenine dinucleotide (FAD)), collagen and elastin, tryptophan, tyrosine and porphyrin, lipofuscins, and melanin [13, 14] display autofluorescence. Because a large number of chromophores exist in organic tissues, it is difficult to identify the fluorescence source. To provide the necessary foundation for the research of an efficient optical diagnosis methodology based on static and time-fluorescence spectroscopy, it is essential to study the absorption, emission, and excitation spectra of thyroid tissues. Therefore, this study aimed to investigate the optical characteristics of ex-vivo thyroid tissues, to produce groundwork and obtain preliminary data on the pathological and physiological alterations of the thyroid tissue.

Methods

Sample Preparation

This study employed 17 human thyroid samples acquired from the University Hospital of the Ribeirão Preto Medical School, University of São Paulo. It included nine patients, from both genders, who presented thyroid diseases and had undergone surgery. The Ethics Committee of the University Hospital of the Ribeirão Preto Medical School, University of São Paulo, approved the study and all the participants signed a written informed consent.

The thyroid samples were removed during surgery, kept in phosphate-buffered saline, and promptly submitted to optical measurements. All the measurements were performed less than 2 h after the surgical procedure. The surgical extraction was performed to provide small samples that were mostly homogeneous. Each sample was bisected: half was used for optical measurement and the other half for pathological analysis. The latter revealed that four, ten, and three of these samples corresponded to healthy, goiter, and papillary carcinoma thyroid tissues, respectively.

As for the optical measurement, the entire half of the selected piece was measured by time-resolved fluorescence spectroscopy. Due to equipment limitations, for the absorption and static fluorescence measurements, the samples were ground in a freezing process using liquid N2 and Agate Mortar & Pestle Sets [15], suspended in distilled water, and placed in quartz cuvettes. The concentration of the samples was not controlled.

Absorption Spectroscopy

The absorption measurements were performed on an array spectrophotometer Amersahm-Pharmacia 2100 Ultraspec at 1800 nm per minute, from 200 to 900 nm, with 1-nm steps. Only absorbance values lower than four were employed.

Static Fluorescence Spectroscopy

A spectrofluorimeter (F-7000, Hitachi) was used to measure steady state fluorescence, in emission and excitation mode, at 2400 nm per minute, from 200 to 800 nm, with 1 nm steps. Excitation and emission slits of 5 or 10 nm were used according to the fluorescence intensity of the sample. The fluorescence spectra were recorded at excitation wavelengths of 285, 290, 300, 365, 410, 525, 575, and 600 nm. Excitation spectra were registered at emission wavelengths of 715, 525, 475, 350, 340, and 300 nm.

Time Resolved Fluorescence Spectroscopy

The fluorescence intensity decay was measured based on time-correlated single photon counting (TSPC). The excitation source was a Tsunami 3950 Spectra Physics titanium–sapphire tunable laser, which emitted wavelengths between 840 and 1000 nm and 6 ps pulses, pumped by the solid-state laser Millenia X Spectra Physics with emission at 530 nm. The pulse repetition rate was set to 8 MHz with the aid of a 3980 Spectra Physics pulse picker. The laser was tuned so that a second- and third-harmonic generator (GWN-23PL Spectra Physics) gave emergent beams in the ranges of 420–500 and 280–333 nm, respectively. The output pulses were coupled to the optical fiber of a fluorescence probe (R400-7-UV–vis, Ocean Optics), and the probe tip was positioned above the selected sample with a gap of approximately 1 mm. The six-fiber bundle of the probe collected the fluorescence and directed the signal to an Edinburgh FL900 spectrometer. The emitted photons were detected by a refrigerated Hamamatsu R3809U

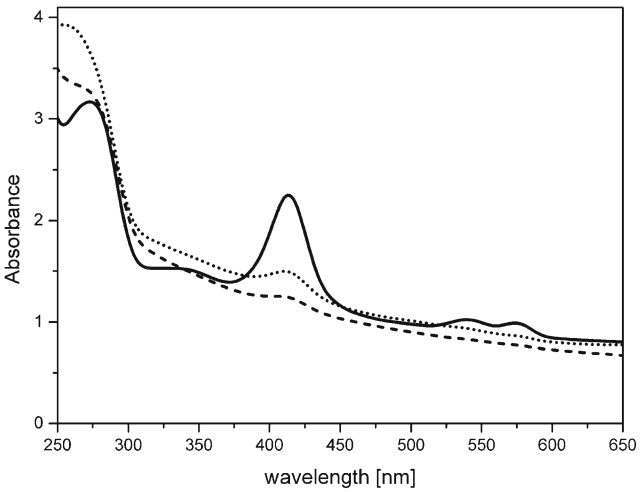

Fig. 1 Absorbance spectra of healthy (——), goiter (– – –), and papillary carcinoma (•••) thyroid tissue samples

Table 1 Peak positions for thyroid absorption measurements in the case of healthy, goiter, and papillary carcinoma samples

Diagnostic	Absorption peaks (nm)				
Healthy	284±2	341±2	414±0	540±1	577±1
Goiter	280±2	340±2	415±0	541±1	578±2
Papillary carcinoma	284±4	342±2	415±0	541±1	577±0

microchannel plate photomultiplier. The software provided by Edinburgh Instruments was used to analyze the decays, by fitting to multiexponential curves.

Samples were excited at 300 nm; the fluorescence intensity decay was registered at 340 and 450 nm, to evaluate the tryptophan and the NAD-H fluorescence, respectively. The high fluorescence intensity at 340 nm delivered decay times for all the samples. However, the low fluorescence intensity at 450 nm prevented us from obtaining reliable decay times for every sample at this wavelength.

Each sample was measured at three different sites, and the fluorescence lifetime was obtained for each of these three measurements. Therefore, we obtained a set of twelve, thirty, and nine lifetimes for the 340 nm emission corresponding to healthy, goiter, and papillary carcinoma thyroid tissues, respectively.

Data Processing

Analyses to determine the peak positions on each spectrum was performed by using smoothing (ten points advanced average) and second derivative (second derivative with ten points Savitzky-Golay smoothing) to distinguish between all the absorption, fluorescence, and excitation peaks. The standard deviation was calculated for each peak position.

All the fluorescence lifetimes values were obtained by tail fitting with two exponential functions. The differences in the lifetimes $\tau 1$ and $\tau 2$ between different tissues (healthy, goiter, and papillary carcinoma) were analyzed by one-way analysis of variance (ANOVA) using the Tukey method.

Results

Optical Absorption

Between 200 and 900 nm, the evaluated thyroid tissues presented absorption bands in three distinct regions. An intense absorbance band emerged between 250 and 300 nm, a second less intense band appeared near 410 nm, and two bands with low intensity arose between 520 and 600 nm. Figure 1 shows the absorption spectrum of three different samples of thyroid tissue: healthy, goiter, and papillary carcinoma.

A peak at 341 nm and peaks at 540 and 577 nm were also discernable. Table 1 lists the average values of the five peaks for the healthy, goiter, and papillary carcinoma samples. The difference between the peaks values obtained for the three groups of samples was very small.

Fluorescence Spectroscopy

The thyroid tissue displayed fluorescence peaks at all the eight different excitation wavelengths (285, 290, 300, 365, 410, 525, 575, and 600 nm), as illustrated in Fig. 2.

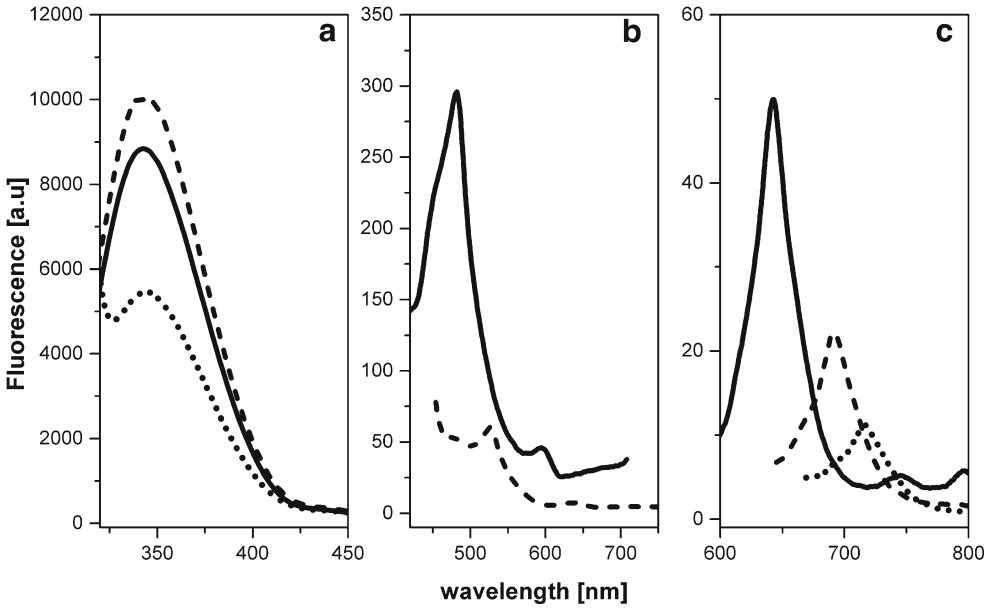

Fig. 2 Fluorescence of a healthy thyroid tissue excited at (a) 285 (——), 290 (– – –) and, 300 nm (•••); (b) 365 (——) and 410 nm (– – –); (c) 525 (——), 575 (– – –), and 600 nm (•••)

Table 2 Fluorescence peak positions for healthy, goiter, and papillary carcinoma thyroid samples

Diagnostic	Fluorescence Peaks (nm)							
	λ_{ex}=285	λ_{ex}=290	λ_{ex}=300	λ_{ex}=365	λ_{ex}=410	λ_{ex}=525	λ_{ex}=575	λ_{ex}=600
Healthy			341±2	449±2			691 ±	716 ±
	343±2	349±0		483±1	532±7	641±1		
	447±0	459±8		596±1	642±3	747±2		
Goiter			341±1	446±3	529±3		691±1	715±1
	343±1	348±2		484±3	641±1*	641±1		
	446±1	466±6		596±1	716±1*	740±8		
Papillary Carcinoma			342±1	446±1			691±0	716±0
	344±1	350±0		482±1	526±1	641±0		
	447±0	472±0		596±1	633±2	738±2		

*These two peaks did not appear together

The sample excited in the region of 285–300 nm presented the highest fluorescence intensity and center at 340 nm. Excitation at 285 and 290 nm enabled identification of peaks close to 340 and 450 nm.

The fluorescence spectrum acquired for the sample excited at 365 nm presented a different profile: a band appeared at 480 nm, accompanied by bands at 449 and 596 nm. Peak analyses of the fluorescence spectrum confirmed these bands.

The fluorescence spectrum for a sample excited at 410 nm exhibited two bands with maximum at 532 and 642 nm, which sometimes shifted to 716 nm. The fluorescence that resulted from excitation at 525, 575, and 600 nm presented two peaks at 641 and 747 nm, one peak at 691 nm, and one peak at 715 nm, respectively.

Table 2 compares the fluorescence peak values for the healthy, goiter, and papillary carcinoma samples.

Excitation Spectroscopy

We acquired the excitation spectra of the thyroid tissue at six different fixed emission wavelengths: 330, 340, 350, 475, 525, and 715 nm. Figure 3 displays the spectra for healthy tissues. When we fixed the emission at 330, 340, and 350 nm, the spectra were similar and presented a peak at 296 nm (Fig. 3a). According to Fig. 3b, at a fixed emission of 475 nm, the spectrum displayed one peak with maximum at 366 nm. The spectrum recorded at fixed emission of 525 nm exhibited a broad band from 350 to 500 nm, with maximum at 443 nm. The spectrum registered at fixed emission of 715 nm displayed two bands, centered at 604 and 296 nm (not shown in Fig. 3). The excitation spectra acquired at fixed emission of 475, 525, and 715 nm presented peaks of low intensity as compared with the spectra recorded at emission of 330, 340, and 350 nm.

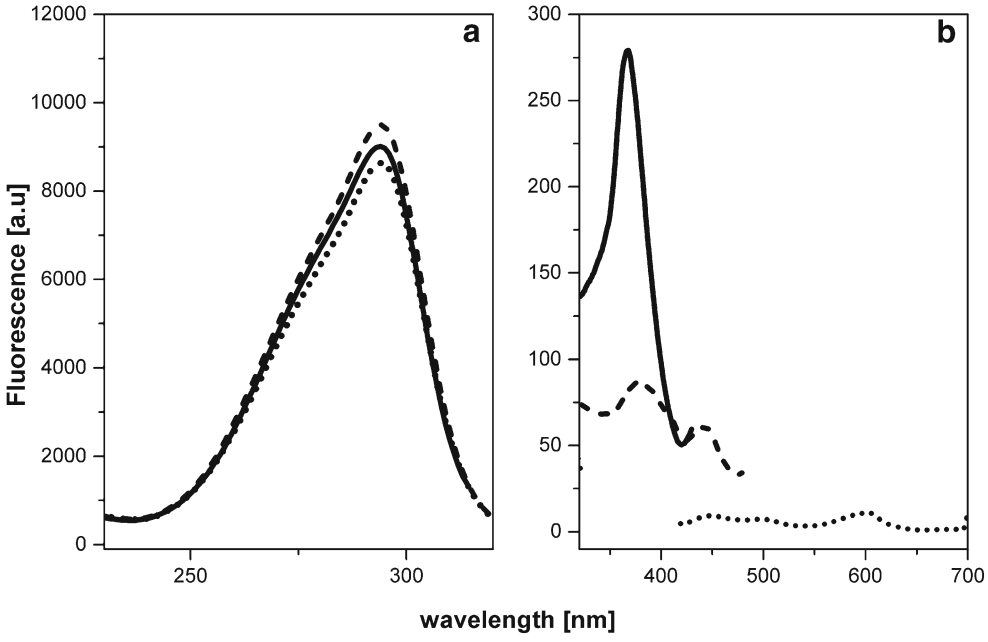

Fig. 3 Excitation spectra of the healthy thyroid tissue sample. On the left (a), the emission recorded at 330 (——), 340 (– – –), and 350 nm (•••) are presented. On the right (b), one can find the peaks for different emissions recorded at 475 (——), 525 (– – –), and 715 nm (•••)

Table 3 Excitation peak positions for healthy, goiter, and papillary carcinoma thyroid samples

Diagnostic	Excitation peaks (nm)					
	λ_{em}=330	λ_{em}=340	λ_{em}=350	λ_{em}=475	λ_{em}=525	λ_{em}=715
Healthy	296±0	296±0	297±1	366±1	443±2	296±1 604±1
Goiter	293±2	296±4	293±3	365±2	446±3	292±2 604±1
Papillary Carcinoma	298±2	298±2	298±2	366±1	443±1	297±2 605±1

Table 3 summarizes the peak values of the excitation spectra of all the samples of thyroid tissue evaluated in this work (healthy, goiter, and papillary carcinoma).

Time-Resolved Fluorescence

Figure 4 contains the time-resolved fluorescence emission for the fresh healthy, goiter, and papillary carcinoma thyroid tissue samples excited at 298–300 nm, measured at 340 nm. The initial delay (about 23 ns) in the measurements was due to the fiber probe and acquisition system.

We fitted each individual fluorescence decay to a bi-exponential curve with a short lifetime close to 1.0 ns and a long lifetime around 4.0 ns. From the set of lifetimes corresponding to a given class of tissue (healthy, goiter, or papillary carcinoma), we calculated the mean values of the short and the long lifetimes (Table 4). We performed analysis of variance using the Tukey method for grouping information with individual confidence level of 98.06 %. For both lifetimes, a statistical difference existed between the healthy tissue and carcinoma, but not between the healthy tissue and goiter. For the two columns labeled 'ANOVA group' in Table 4, the same letters mean non-statistical difference.

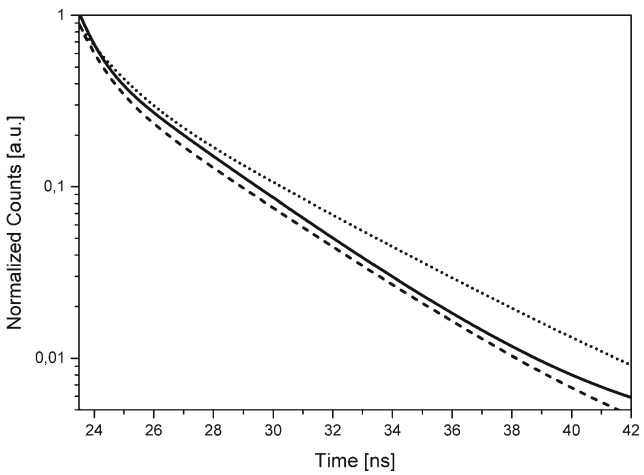

Fig. 4 Normalized time-resolved fluorescence measurements at 340 nm for healthy (——), goiter (– – –), and papillary carcinoma (•••) thyroid tissue samples excited at 300 nm

Discussion

The present results comprise absorbance, fluorescence, excitation, and time-resolved fluorescence measurements and constitute a first approach to establish a fluorescence-based diagnostic method for thyroid tissues.

The absorbance, fluorescence, and excitation results aided detection of fluorophores in the thyroid samples by means of peaks analyses. The largest absorption band centered at 284 nm refers mostly to the presence of elastin and tryptophan in the tissue [12, 14, 16, 17]. The highest fluorescence intensity at around 340 nm, achieved by exciting the sample in the 285–300 nm region, also corresponds to the tryptophan fluorescence [13, 14].

For the fluorescence acquired by exciting the sample at 365 nm, the bands at approximately 449, 483, and 596 nm indicate the presence of elastin, lipofuscin, NADH-protein, and NADH-free [13, 14, 16, 17]. The emission at 475 nm gives an excitation peak at about 365 nm, which also indicates excitation wavelength consistent with the presence of NADH [13, 17].

The absorption band centered at 410 nm lies within the region where several chromophores absorb; e.g., photoporphyrin, hemoglobin and Flavin adenine dinucleotide (FAD) [13, 14, 16, 17]. The fluorescence spectra for the samples excited at 410 nm display emission bands at approximately 532 and 641 nm, consistent with FAD (free and protein-bound), flavinmonocleotide (FMN), riboflavin, and protoporphyrin IX fluorescence [14–17]. Additionally, samples

Table 4 Fluorescence time decay for the healthy, goiter, and papillary carcinoma thyroid samples excited at 300 nm and measured at 340 nm, and analysis of variance (ANOVA) results

Diagnostic	τ_1		τ_2	
	Average decay time (ns)	ANOVA group*	Average decay time (ns)	ANOVA group*
Healthy	0.81±0.22	A	3.93±0.40	A
Goiter	0.76±0.17	A	3.64±0.32	A
Papillary Carcinoma	1.22±0.21	B	4.81±0.40	B

*Same letters denote non-statistical difference – comparison performed for each column

emitting at 525 nm present excitation bands at 443 nm, which is also consistent with the excitation wavelengths for NADH, protoporphyrin, FAD (free and protein bound), FMN, and riboflavin [13, 14, 16, 17]. The fluorescence resulting from the excitations at 525, 575, and 600 nm present peaks, which emerge around 641, 691, and 716 nm respectively, could also be due to the presence of protoporphyrins [13, 17].

As expected, the observed bands and tissue constituents are similar to those reported in the literature [8, 10, 13, 14, 16, 17] for soft tissues; however, thyroid tissues can also present thyroglobulin and iodine. The optical characteristics of fluorophores depend on the properties of the medium, such as pH and temperature, and their ligands. Hence, it is not possible to compare the lifetime fluorescence observed for thyroid samples directly with those of other tissues, even though the chromophore constituents are similar [13, 14, 16, 17]. In addition, it is very difficult to establish which fluorophore(s) is responsible for the differences in lifetime with this technique.

The lifetime of tryptophan in neutral aqueous solution for emission at 340 nm is 0.67±0.12 and 3.17± 0.04 ns [18–20]. However, many factors affect tissue autofluorescence, reflecting the complexity of biological systems. The time-resolved fluorescence measurements for the healthy thyroid samples at 340 nm yielded lifetimes of 0.81±0.2 and 3.93±0.4 ns. Additionally, it is noteworthy that carcinoma samples have larger lifetimes. Recent studies have connected cancer with activation of systemic tryptophan metabolism, so that the malignancy evades immune control. Which also suggests that tryptophan catabolism may serve as a biomarker to monitor disease activity and response to therapy in cancer patients [21–23]. The tryptophan metabolic pathway could be the cause for these longer fluorescence lifetimes. However, further studies are still necessary to determine whether lifetime values can consistently distinguish between thyroid malignant lesions and healthy thyroid tissue.

Conclusions

This study is an initial investigation on the optical characteristics of thyroid tissues with a small dataset. It has successfully demonstrated that thyroid fluorescence originates from many fluorophores and culminates in several bands. It also revealed different lifetimes for samples with carcinoma, suggesting that these characteristics can potentially assist diagnosis. Fluorescence spectroscopy and time-resolved fluorescence are the most promising techniques for application in medical diagnosis, because they employ optical fiber probes and are minimally invasive. Therefore, it is important to investigate fluorescence bands and lifetimes, to identify differences between normal and pathological thyroid tissues. Future studies and a larger set of samples are necessary to elucidate the correlation between the fluorescence peaks and lifetimes for all thyroid pathologies.

Acknowledgments The authors would like to acknowledge Universidade de São Paulo – USP, Fundação de Amparo à Pesquisa do Estado de São Paulo – FAPESP (Projects number 2011/07960-4 and 2012/02460-6), and Conselho Nacional de Desenvolvimento Científico e Tecnológico – CNPq (Project number 160014/2012-3) for the grants and fellowships given to this research. The authors thank Cynthia Maria de Campos Prado Manso for linguistic advice.

References

1. Rout P, Shariff S (1999) Diagnostic value of qualitative and quantitative variables in thyroid lesions. Cytopathology 10(3):171–179
2. Teixeira CS et al (2009) Thyroid tissue analysis through Raman spectroscopy. Analyst 134(11):2361–2370
3. Zhang X et al (2011) Intraoperative detection of thyroid carcinoma by Fourier transform infrared spectrometry. J Surg Res 171(2):650–656
4. Gupta N et al (2011) Evaluation of the role of magnetic resonance spectroscopy in the diagnosis of follicular malignancies of thyroid. Arch Surg 146(2):179–182
5. Suh H et al (2011) Elastic light-scattering spectroscopy for discrimination of benign from malignant disease in thyroid nodules. Ann Surg Oncol 18(5):1300–1305
6. Chen X et al (2012) Quantitative analysis of collagen change between normal and cancerous thyroid tissues based on SHG method. Proc SPIE 8329:83290H
7. Zhou C et al (2010) Ex vivo imaging of human thyroid pathology using integrated optical coherence tomography and optical coherence microscopy. J Biomed Opt 15(1):016001–1–016001–9
8. Pitman MJ et al (2004) The fluorescence of thyroid tissue. Otolaryngol Head Neck Surg 131(5):623–627
9. Ebenezar J et al (2012) Noninvasive fluorescence excitation spectroscopy for the diagnosis of oral neoplasia in vivo. J Biomed Opt 17(9): 97007–1
10. Giubileo G et al (2005) Fluorescence spectroscopy of normal and follicular cancer samples from human thyroid. Spectrosc 19(2):79–87
11. Paras C et al (2011) Near-infrared autofluorescence for the detection of parathyroid glands. J Biomed Opt 16(6):067012–1–067012–4
12. Uehlinger P et al (2009) In vivo time-resolved spectroscopy of the human bronchial early cancer autofluorescence. J Biomed Opt 14(2): 024011
13. Berezin MY, Achilefu S (2010) Fluorescence lifetime measurements and biological imaging. Chem Rev 110(5):2641–2684
14. Marcu L (2012) Fluorescence lifetime techniques in medical applications. Ann Biomed Eng 40(2):304–331
15. Chan E, Menovsky T, Welch AJ (1996) Effects of cryogenic grinding on soft-tissue optical properties. Appl Optics 35(22):4526–4532
16. Bachmann L et al (2006) Fluorescence spectroscopy of biological tissues—a review. Appl Spectrosc Rev 41(6):575–590
17. Chorvat D Jr, Chorvatova A (2009) Multi-wavelength fluorescence lifetime spectroscopy: a new approach to the study of endogenous fluorescence in living cells and tissues. Laser Phys Lett 6(3):175–193

18. Rayner DM, Szabo AG (1978) Time resolved fluorescence of aqueous tryptophan. Can J Chem 56(5):743–745
19. Engelborghs Y (2001) The analysis of time resolved protein fluorescence in multi-tryptophan proteins. Spectrochim Acta 57(11):2255–2270
20. Goldman C, Pascutti PG, Piquini P, Ito AS (1995) On the contribution of electron transfer reaction to the quenching of tryptophan fluorescence. J Chem Phys 103:10614–10620
21. Platten M, Wick W, Van den Eynde BJ (2012) Tryptophan catabolism in cancer: beyond IDO and tryptophan depletion. Cancer Res 72(21):5435–5440
22. Opitz CA et al (2011) An endogenous tumour-promoting ligand of the human aryl hydrocarbonreceptor. Nature 478(7368):197–203
23. Liu X et al (2010) Selective inhibition of IDO1 effectively regulates mediators of antitumor immunity. Blood 115(17):3520–3530